Available online www.jocpr.com

Journal of Chemical and Pharmaceutical Research, 2014, 6(10):263-273

Research Article

ISSN : 0975-7384
CODEN(USA) : JCPRC5

Image segmentation framework using directional gradient guided LBF

Bo Cai[1,2*], Zhigui Liu[1,2] and Yuyu Zhu[1]

[1]Southwest University of Science & Technology, Mianyang Sichuan, China
[2]China Academy of Engineering Physics, Mianyang, Sichuan, China

---

ABSTRACT

Image segmentation is a fundamental and challenging problem in image processing and often a vital step for high level analysis. Considering of the inefficient curve evolution against weak boundary and intensity heterogeneous images, an improved level set segmentation framework based on image directional gradient is proposed. In this framework, we divide the evolution processing into two stages: the evolution of the image background and foreground, and the evolution of the image regions based on the chosen directional gradient. Compare to the other local information based active contour evolution algorithm: Local Binary Fitting (LBF) model, this algorithm may improve efficient of curve evolution in a large extent. Extensive experiments on synthetic and real images are provided to evaluate our method, showing the segmentation of the blurry boundary and intensity heterogeneous images may achieve more accuracy results.

Keywords: Image segmentation; CV model; Directional Gradient; LBF

INTRODUCTION

Image segmentation as the subject of intensive research and a wide variety of segmentation techniques has been reported in recent decades. Active Contour Model (ACM) based segmentation algorithm has been widely investigated and applied to the image segmentation [1-8]. In general, the basic idea of active contour model is to deform an initial contour toward the actual boundary of the object.

Active Contour Model based algorithms may be categorized into edge-based[3, 9] and region based[1, 5, 6, 10, 11] models. In edge and region based ACM, image gradient and statistical information are often used to stop the contours respectively. The benefit of the model is that the image has no global constraints, thus the objective and the background can be heterogeneous and the final segmentation can be achieved easily. However, the method relies heavily on edge information of the input image, when an edge of the region is weak, such as blurred, or broken, the method may loss its roll.

Region-based active contour model (ACM) utilizes the objective and the background regions statistically and finds an energy optimum where the model best fits the image. Because of more advantages over edge-based ACMs, such as robustness for image with weak edges or without edges and insensitivity to the location of initial contours, region-based ACMs have been applied more popularly, in which, the Chan-Vese (CV) model[12] is one of the most popular region-based models. However, techniques that attempt to model regions using these kinds of methods are usually not ideal for segmenting heterogeneous objects, or transitional regions, which frequently occur in natural images.

There are many methods in the literature which are aimed at improving the segmentation accurate by introducing more edge or region information into the active contour model. Because of the minimization of the energy function heavily depends on the gray scale and the distribution and area of the image regions, the total information often

leads to the false segmentation in the local region of the image. To overcome the problem of region non-homogeneous, Ge Qi et al[11] proposed a region based model with an anisotropic region fitting energy represented by a variational energy function. They introduced a structure tensor to define an anisotropic region fitting energy functional so that the intensity of an observed pixel is approximated through the intensity of its adjacent pixels at the principal directions. For the purpose of letting the active contour model more conform to the edges of the image region, Kovacs, Andrea et al[13] generates the main feature points based on the Harris corner detector, then these points are enveloped to get the initialization of the contour. Faced on the problems of intensity inhomogeneity, Yang, Yunyun et al[14] divide the fitting energy as local intensity fitting (LIF) energy and global intensity fitting (GIF) energy, and then use the two terms RSF model and CV model to realize the minimization of local-global intensity energy function. Since the external force plays a leading role in driving the active contour models, designing a novel external force field has been extensively studied [1, 5, 9, 10, 15]. Among all these external forces, gradient, edge, and gradient vector flow (GVF) has been used by Zhou Huiyu et al [16] as the outer driven force. In [9], Fang Lingling et al using the EdgeFlow-Based (EFB) active contour to realize the segmentation of the heterogeneous regions. Because of the edge of the regions is difficult to get, they use the Gaussian Mixture Model to realize the initial contour.

In this paper, we focus on the combining of the edge and region information in the evolution of active contour model. For the purpose of letting the region characterization be considered into the evolution, we use the image directional gradient as the guided direction and resampling the evolution result of each step. The main advantages of our segmentation method can be highlighted as:

(1) Due to the resampling guided by the directional gradient, the regions of the evolution result become more homogeneous than the other active contour models. In fact, for all of the active contour model algorithms, the evolution processing is aimed at finding out an approximate image which is more easily to be segmented and at the same time the segmentation results is agree to the disposed image. The more homogenous the region is, the more accuracy the contour would be achieved.

(2) Because of the resampling processing is guided by the pre-calculated directional gradient, there is no parameters needed to be decided. It makes the algorithm more flexible in processing different images.

The remainder of this paper is organized as follows. In section 2, we give briefly review the local binary fitting (LBF) [17] model and some other ACM based models. The proposed model is introduced in section 3. In section 4, the role of different directional gradient algorithms has been compared in our proposed model. Section 5 is the comparison of our model with LGIF, LBF in evolution efficient and segmentation results. We go on analyzing the results when the image is noised. Finally, the conclusion and limitations of our model have been discussed in section 6.

2. The review and discussion of the related works

In this section, we give a review of the related active contour models based on Chan and Vese [12] model. For a given image $I(x)$ on the image domain R , Chan-Vese proposed to minimize the following energy equation:

$$E^{CV}(c_1, c_2, C) = \lambda_1 \int_{in(C)} |I(x) - c_1|^2 \, dx + \lambda_2 \int_{out(C)} |I(x) - c_2|^2 \, dx \tag{1}$$

where c_1 and c_2 are two constants that approximate the average intensity inside and outside the curve, respectively. The coefficients λ_1 and λ_2 are fixed parameters.

In Chan-Vese model, they also have a regularizing term, such as the length of the contour and the area inside and outside the contour to improve the smoothness of the boundary. The energy $E^{CV}(c_1, c_2, C)$ is defined as:

$$\begin{aligned} E^{CV}(c_1, c_2, C) = {} & \lambda_1 \int_{in(C)} |I(x) - c_1|^2 \, dx + \lambda_2 \int_{out(C)} |I(x) - c_2|^2 \, dx \\ & + \mu \text{Length}(C) + \nu \, Area(in(C)) \end{aligned} \tag{2}$$

Using the level set to represent C, that is, C is the zero level set of Lipschitz function $\phi(x)$, the energy function may be rewritten as:

$$\begin{aligned} E^{CV}(c_1,c_2,\phi) &= \lambda_1\int_R |I(x)-c_1|^2 H(\phi(x))dx + \lambda_2\int_R |I(x)-c_2|^2 (1-H(\phi(x)))dx \\ &+\mu\int_R \delta(\phi(x))|\nabla\phi(x)|dx + \nu\int_R H(\phi(x))dx \end{aligned} \tag{3}$$

where $H(\phi)$ and $\delta(\phi)$ are Heaviside function and Dirac function, respectively. The coefficients μ and ν are fixed parameters.

The CV model has a good performance on image segmentation due to its ability of obtaining a larger convergence range and being less sensitive t the initialization. However, the CV model is only adapted for 2-phase image. If the intensities with inside C or outside C are not homogeneous, the constants c_1 and c_2 will not be accurate. To overcome the difficult caused by intensity inhomogeneous, Li et al. proposed the local binary fitting (LBF) model[18], which can utilize the local intensity information. In the LBF model, two spatially varying fitting functions $f_1(x)$ and $f_2(x)$ are introduced to approximate the local intensities on the two sides of the contour, and for a given point $x\in R$, the local intensity fitting energy is defined by

$$\begin{aligned} E_x(C, f_1, f_2) &= \lambda_1\int_{in(C)} g(x-y)(I(y)-f_1(x))^2 dy \\ &+\lambda_2\int_{out(C)} g(x-y)(I(v)-f_2(x))^2 dy \end{aligned} \tag{4}$$

where λ_1 and λ_2 are positive constants, $g(y)$ is a Gaussian kernel function, and $f_1(x)$, $f_2(x)$ are two values that approximate image intensity inside and outside contour C, respectively.

The above local fitting energy $E_x(C, f_1, f_2)$ is defined for a center point x. For all the center point x in the image domain R, the energy function can be defined by

$$\begin{aligned} &E^{LBF}(C, f_1(x), f_2(x)) \\ &= \int_R E_x(C, f_1(x), f_2(x))dx \\ &= \lambda_1\int_R \left[\int_R g(x-y)(I(y)-f_1(x))^2 H(\phi(y))dy\right]dx \\ &+\lambda_2\int_R \left[\int_R g(x-y)(I(v)-f_2(x))^2 (1-H(\phi(y)))dy\right]dx \end{aligned} \tag{5}$$

Another way to deal with the intensity discontinuity is use the edge information as the factor of the ACM model. Fang et al. [19] define the energy function $x\in R$ as

$$
\begin{aligned}
&E_x^{EFB} = \int_{in(C)} g(y)\left|I(y)-c_1\right|^2 dy \\
&+\int_{out(C)} g(y)\left|I(y)-c_2\right|^2 dy + \lambda\int_R \delta_\varepsilon(\phi(x))\left|\nabla\phi(x)\right| \\
&= \int_R g(y)\left|I(y)-c_1\right|^2 H_\varepsilon(\phi)\, dy \\
&+\int_R g(y)\left|I(y)-c_2\right|^2 (1-H_\varepsilon(\phi))\, dy \\
&+\lambda\int_R \delta_\varepsilon(\phi(x))\left|\nabla\phi(x)\right|
\end{aligned}
\tag{6}
$$

where $g(y)$ denotes Edge-Flow Based function: $g(y)=1\Big/\left(1+(y/k)^2\right)^m$, k is a contrast parameter separating low-contrast regions from high-contrast edges: $\mathrm{k}=1.4826\times median\left(\left\|y-median(y)\right\|\right)$. They define $median(\cdot)$ as median operation, and use this selective process ensures that the image operation. And this selective process ensures that the image region is for $y<k$ and the image edge is for $y\geq \mathrm{k}$. Besides, m is a regulatory factor of Edge-Flow based function, which can achieves a better balance between keeping region edge and remove the noise near the edge.

Following this way, there are some papers aimed at dividing the local characters and the global characters of the image [3-5, 15, 20, 21], and constructing the energy function to solve the global and local problems. In this paper, we'll following the visual processing of the image to deal with the local and problems. As stated in [19], the global contrast and local contrast is the key reference in human visual processing. Commonly, the high contrast of the image is related to the edge of the image regions. However, the edges are often exists in the different phase of image regions, and make the edges inhomogeneous in local regions. Simply sum the difference of all local regions may cause the global optimizing function result inconsistence to the local dividing results. On the other hand, only using the local dividing result to approximate the global segmentation may cause the wrong segment of the transitional regions and the parameter is difficult to choose.

In this paper, we focus on the role of the image gradient and the global/local contrast in the active contour model (ACM) iteration. According to our experiments, the global mean c_1 and c_2 is the classification center of the image gray, and their value are mainly influenced by the total inner region pixels instead of the edge pixels. Comparing to the inner gray distribution, the contour is more easily influenced by the edge pixels' gray. At the same time, because of the inhomogeneous of the region edges, the dividing of different region may exist or not exist in the difference between c_1 and c_2. When the edge-grays of the region are all less or higher than the global center c_1 and c_2, the global dividing reference may lose its role.

3. The proposed model

3. 1 The local binary fitting model

Given the input image $I(x)$ on the image domain R, LBF model use the region-based intensity information as a controllable scale in the energy model.

$$
\begin{aligned}
&E^{LBF}\left(C, f_1(x), f_2(x)\right) \\
&= \int_R E_x\left(C, f_1(x), f_2(x)\right) dx \\
&= \lambda_1\int_R\left[\int_R g(x-y)\left(I(y)-f_1(x)\right)^2 H(\phi(y))\, dy\right] dx \\
&+\lambda_2\int_R\left[\int_R g(x-y)\left(I(\mathrm{y})-f_2(x)\right)^2 (1-H(\phi(y)))\, dy\right] dx
\end{aligned}
\tag{7}
$$

The nonnegative weighted kernel function $g(x-y)$ is chosen as the Gaussian function $g(u)=\frac{1}{(2\pi)^{n/2}\sigma^n}e^{-|u|^2/2\sigma^2}$. Where $H(\phi)$ and $\delta(\phi)$ are Heaviside function and Dirac function respectively. Generally, the regularized versions are selected as

$$\begin{aligned} H_\varepsilon(z)&=\frac{1}{2}\left(1+\frac{2}{\pi}\arctan\left(\frac{z}{\varepsilon}\right)\right)\\ \delta_\varepsilon(z)&=\frac{1}{\pi}\frac{\varepsilon}{\varepsilon^2+z^2},\quad z\in R \end{aligned} \tag{8}$$

In LBF model, they keep the $\phi(x)$ fixed, and minimizing the energy $E^{LBF}(\phi,c_1,c_2)$ with respect to the constant $c_1=f_1(x)$ and $c_2=f_2(x)$ by using Euler-Lagrange equations. The calculation of c_1 and c_2 may be obtained:

$$\begin{cases} c_1(\phi)=\dfrac{\int_R g(x)*\left[I(x)H(\phi(x))\right]dx}{\int_R g(x)*H(\phi(x))dx}\\ c_2(\phi)=\dfrac{\int_R g(x)*\left[I(x)(1-H(\phi(x)))\right]dx}{\int_R g(x)*(1-H(\phi(x)))dx} \end{cases} \tag{9}$$

Here, c_1 and c_2 are the weighted means of the foreground and background of the image.

3. 2 The gradient guided algorithm

In LBF model, the weighted coefficient $g(x-y)$ is used to dispose the local characterization of the image. But the calculation of c_1 and c_2 is based on the evolutionary contour, the more homogeneous the inner region pixels the more quickly the edge would be achieved and at the same time the edge would be more accuracy. So, in this section, we consider the homogeneous of the evolution processing according to the image gradient.

The definition of the image segmentation may be defined as, given image $I(x)$ in the image domain R, if we want to segment it into N classes $R_i,\quad i=1,\ldots,N$, then it should the following two conditions:

$$\begin{cases} R=\bigcup_{i=1}^{N}R_i\\ R_i\bigcap_{i\neq j}R_j=\Phi \end{cases} \tag{10}$$

From the above definition, we may found that all of the pixels of the image should belong to one and only one class $R_i, i\in\{1,\cdots,N\}$. If we omitted the single pixel or small pixel regions, then for any pixel of the image there must exist the connected class the pixel should belong to. Based on the assumption, we construct the gradient guided resampling of the region inner pixels. For any image, the gradient information is most near to the image region edges, but the choosing of the threshold of image gradient as the region edge is very difficult because of the inhomogeneous of the region edges. For the purpose of avoiding the choosing of the threshold, we choose the region information as the homogeneous algorithm of the evolution processing.

On this condition, we transfer the edge problem into the pixel and region merge problem. To decide which region the pixel should belonging, we calculate the directional gradient of each pixel as following eight directional template $T_i, i=1,\ldots,8$. The absolute smallest directional gradient is the pixel should belong to.

$$\begin{bmatrix} 0 & 0 & 0 & 0 & 0 & 0 & 0 \\ 0 & 0 & 0 & 0 & 0 & 0 & 0 \\ 1/9 & 1/9 & 1/9 & 0 & 0 & 0 & 0 \\ 1/9 & 1/9 & 1/9 & -1 & 0 & 0 & 0 \\ 1/9 & 1/9 & 1/9 & 0 & 0 & 0 & 0 \\ 0 & 0 & 0 & 0 & 0 & 0 & 0 \\ 0 & 0 & 0 & 0 & 0 & 0 & 0 \end{bmatrix}, \begin{bmatrix} 1/9 & 1/9 & 1/9 & 0 & 0 & 0 & 0 \\ 1/9 & 1/9 & 1/9 & 0 & 0 & 0 & 0 \\ 1/9 & 1/9 & 1/9 & 0 & 0 & 0 & 0 \\ 0 & 0 & 0 & -1 & 0 & 0 & 0 \\ 0 & 0 & 0 & 0 & 0 & 0 & 0 \\ 0 & 0 & 0 & 0 & 0 & 0 & 0 \\ 0 & 0 & 0 & 0 & 0 & 0 & 0 \end{bmatrix}, \begin{bmatrix} 0 & 0 & 1/9 & 1/9 & 1/9 & 0 & 0 \\ 0 & 0 & 1/9 & 1/9 & 1/9 & 0 & 0 \\ 0 & 0 & 1/9 & 1/9 & 1/9 & 0 & 0 \\ 0 & 0 & 0 & -1 & 0 & 0 & 0 \\ 0 & 0 & 0 & 0 & 0 & 0 & 0 \\ 0 & 0 & 0 & 0 & 0 & 0 & 0 \\ 0 & 0 & 0 & 0 & 0 & 0 & 0 \end{bmatrix}, \begin{bmatrix} 0 & 0 & 0 & 0 & 1/9 & 1/9 & 1/9 \\ 0 & 0 & 0 & 0 & 1/9 & 1/9 & 1/9 \\ 0 & 0 & 0 & 0 & 1/9 & 1/9 & 1/9 \\ 0 & 0 & 0 & -1 & 0 & 0 & 0 \\ 0 & 0 & 0 & 0 & 0 & 0 & 0 \\ 0 & 0 & 0 & 0 & 0 & 0 & 0 \\ 0 & 0 & 0 & 0 & 0 & 0 & 0 \end{bmatrix}$$

$$\begin{bmatrix} 0 & 0 & 0 & 0 & 0 & 0 & 0 \\ 0 & 0 & 0 & 0 & 0 & 0 & 0 \\ 0 & 0 & 0 & 0 & 1/9 & 1/9 & 1/9 \\ 0 & 0 & 0 & -1 & 1/9 & 1/9 & 1/9 \\ 0 & 0 & 0 & 0 & 1/9 & 1/9 & 1/9 \\ 0 & 0 & 0 & 0 & 0 & 0 & 0 \\ 0 & 0 & 0 & 0 & 0 & 0 & 0 \end{bmatrix}, \begin{bmatrix} 0 & 0 & 0 & 0 & 0 & 0 & 0 \\ 0 & 0 & 0 & 0 & 0 & 0 & 0 \\ 0 & 0 & 0 & 0 & 0 & 0 & 0 \\ 0 & 0 & 0 & -1 & 0 & 0 & 0 \\ 0 & 0 & 0 & 0 & 1/9 & 1/9 & 1/9 \\ 0 & 0 & 0 & 0 & 1/9 & 1/9 & 1/9 \\ 0 & 0 & 0 & 0 & 1/9 & 1/9 & 1/9 \end{bmatrix}, \begin{bmatrix} 0 & 0 & 0 & 0 & 0 & 0 & 0 \\ 0 & 0 & 0 & 0 & 0 & 0 & 0 \\ 0 & 0 & 0 & 0 & 0 & 0 & 0 \\ 0 & 0 & 0 & -1 & 0 & 0 & 0 \\ 0 & 0 & 1/9 & 1/9 & 1/9 & 0 & 0 \\ 0 & 0 & 1/9 & 1/9 & 1/9 & 0 & 0 \\ 0 & 0 & 1/9 & 1/9 & 1/9 & 0 & 0 \end{bmatrix}, \begin{bmatrix} 0 & 0 & 0 & 0 & 0 & 0 & 0 \\ 0 & 0 & 0 & 0 & 0 & 0 & 0 \\ 0 & 0 & 0 & 0 & 0 & 0 & 0 \\ 0 & 0 & 0 & -1 & 0 & 0 & 0 \\ 1/9 & 1/9 & 1/9 & 0 & 0 & 0 & 0 \\ 1/9 & 1/9 & 1/9 & 0 & 0 & 0 & 0 \\ 1/9 & 1/9 & 1/9 & 0 & 0 & 0 & 0 \end{bmatrix}$$

Along with the gradient guided direction, we resample each evolution results using the directional mean value templates. Like the directional gradient templates, we define the weighted directional mean value templates MT_i ($i=1,\ldots,8$) as:

$$\begin{bmatrix} 0 & 0 & 0 & 0 & (1-1/a)/9 & (1-1/a)/9 & (1-1/a)/9 \\ 0 & 0 & 0 & 0 & (1-1/a)/9 & (1-1/a)/9 & (1-1/a)/9 \\ 0 & 0 & 0 & 0 & (1-1/a)/9 & (1-1/a)/9 & (1-1/a)/9 \\ 0 & 0 & 0 & 1/a & 0 & 0 & 0 \\ 0 & 0 & 0 & 0 & 0 & 0 & 0 \\ 0 & 0 & 0 & 0 & 0 & 0 & 0 \\ 0 & 0 & 0 & 0 & 0 & 0 & 0 \end{bmatrix}$$

In the weighted directional mean value templates, when the coefficient $a=10$, the template becomes to the normal directional mean value templates. Otherwise, when $1<a<10$, the center pixel is emphasized. Fig.1 shows the filtered result of the directional gradient.

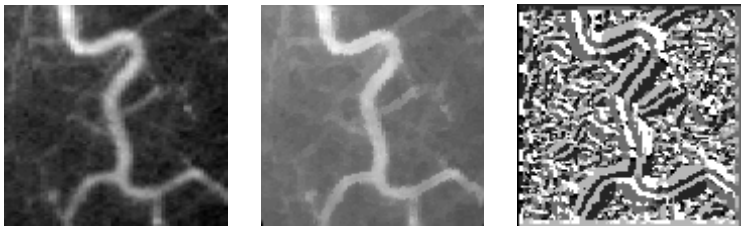

(a) **(b)** **(c)**

Fig 1 The rough image, the image gradient and the guided image gradient

Seeing from the result of the directional gradient of Fig.1(c), the local maximum gradient may influence the homogeneous processing. And at the same time, because of the initial contour may cause the evolution wrongly dividing the foreground and background in the local fitting processing. Fig.2 shows the fault dividing of the evolution processing. For the purpose of punishing the wrong segmentation, in the evolution processing, we use the global mean $\overline{c}_1$ and $\overline{c}_2$ of the image upside and downside gray value as the total reference to punish the wrong segmentation of each evolution.

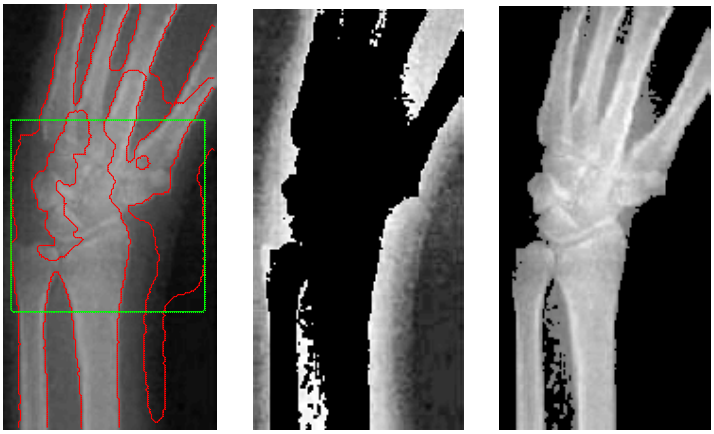

(a) **(b)** **(c)**

Fig 2 (a) is the evolution result of LBF after 100 times, (b) is the down parts of the image gray, (c) is the upper parts of the image gray

3. 3 Level set formulation

In the level set based segmentation method, the segmentation contour c is represented as the zeroth level of a level set function ϕ. We focus on the homogeneous of the level set function ϕ by using the weighted directional mean value template. In such a case, the cluster member is set to 2. The homogeneous processing produce the new level set ϕ' after each evolution step, and the two class center c_1 and c_2 may be calculated as ep.13.

$$\phi'(x) = MT_k(x) * \phi(x) \quad (12)$$

$$\begin{cases} c_1'(\phi) = \dfrac{\int_R g(x) * \left[I(x) H(\phi'(x)) \right] dx}{\int_R g(x) * \left[H(\phi'(x)) \right] dx} \\ c_2'(\phi) = \dfrac{\int_R g(x) * \left[I(x) \left(1 - H(\phi'(x))\right) \right] dx}{\int_R g(x) * \left[\left(1 - H(\phi'(x))\right) \right] dx} \end{cases} \quad (13)$$

where $MT_k(x)$ is the absolute minimum gradient direction of the image pixel $\mathrm{k} = \left\{ \min\left(abs\left(T_k(x) \right) \right) | k = 1, \ldots, 8 \right\}$.

To preserve the regularity of the level set function ϕ, which is necessary for accurate computation and stable level set evolution, we introduce a level set regularization term in the variational level set formulation. The level set regularization term is defined as:

$$L(\phi) = \mu \int_R \left| H(\phi(x)) \right| dx \quad (14)$$

Adding the length term into the total energy function:

$$\begin{aligned} & E(C, c_1', c_2') \\ & = \int_R E_x(C, c_1', c_2') dx + \mu \int_R \left| H(\phi'(x)) \right| dx \\ & = \lambda_1 \int_R \left[\int_R g(x-y) \left(I(y) - c_1' \right)^2 H(\phi'(y)) dy \right] dx \\ & + \lambda_2 \int_R \left[\int_R g(x-y) \left(I(\mathrm{y}) - c_2' \right)^2 \left(1 - H(\phi'(y))\right) dy \right] dx \\ & + \mu \int_R \left| H(\phi'(x)) \right| dx \end{aligned} \quad (15)$$

where λ_1, λ_2 and u are the constant coefficient.

3. 4 Optimization of the model

For the purpose of letting region information guide the iteration, we divide the image into two parts, region inner area and region edge area. Before the calculation of the background mean and foreground mean, we use the directional mean value template to resample the region inner pixels of $\phi(x)$. After the resampling processing, we keep c_1' and c_2' fixed, and then to minimize the energy function $E(C, c_1', c_2')$. Parameterizing the descent direction by an artificial time t, we can obtain the corresponding variational level set function.

Keeping the clusters c_1' and c_2' fixed, the level set function is updated by solving the gradient flow equation:

$$\phi^t = \phi^{t-1} - \eta \frac{dE\left(\phi, c_1', c_2'\right)}{d\phi} \tag{16}$$

where η is the time step.

$$\begin{aligned} &\frac{\partial \phi'(x,t)}{\partial t} \\ &= \delta(\phi')\left[-\lambda_1\left(I(x)-c_1'\right)^2 + \lambda_2\left(I(x)-c_2'\right)^2\right] \\ &+\delta(\phi')\left[\mu div\left(\frac{\nabla\phi'}{|\nabla\phi'|}\right) - \upsilon\right] \end{aligned} \tag{17}$$

Because of the image gradient has been used to guide resampling in the iteration processing, specifically the region inner pixels, the iteration processing is able to make the region inner pixels more smoothly, and at the same time it accelerate the evolution. As a result, it makes the energy more similar to the region contours, the time consumption is also heavily decreased.

4. Implementation and experimental results

In order to demonstrate the strengths of the proposed model, we perform different kinds of experiments. First of all, we compare the proposed model segment results with the other local based ACM model such as LBF. Secondly, we continue with the properties of the proposed model with various images, and analyze the corresponding number of iterations and time. Finally, we'll give the analysis of the guided gradient extraction with different coefficients.

4.1 Comparison with other local based ACM models

Commonly, the accurate choose of initial contour is an important part in the process of image segmentation. In our model, the resampling of the inner region has the ability of dealing with the wrongly initialize contour, as a result, it may leads the iteration convergence to the correct edge of the image. Firstly, we will give the comparison of the different initial contour of different algorithms. In this experiment, we choose two kinds of initial contours (the edge included initial contour and none edge initial contour) by hand. For the iteration times, we set it as 300. Fig.3 shows the results of the proposed model with different initial contour.

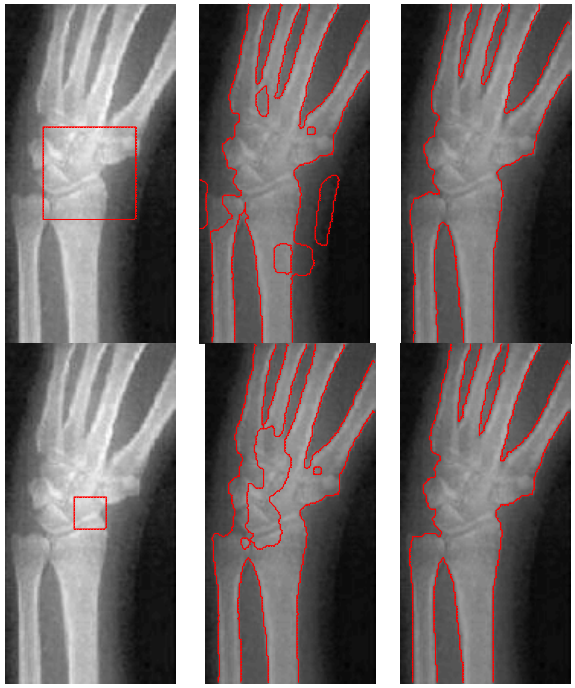

Fig.3 The iteration results of different model, the first column is the rough image and the initial contour, the second column is the result of LBF, and the third column is the proposed result. (In all the experiments, we let the sigma as a constant value 4, the iteration times is 300)

4.2 The corresponding number of iterations

In this section, we give compare the corresponding energy value of the proposed algorithm and the other local based active contour models. For the purpose of compare the convergence of the energy values, we scale the total energy and give the curve of different models. Because of the initial contour of different model may causing different results, we choose the correct initial contour with different model to compare the convergence. Fig.4 shows the convergence processing between each evolution.

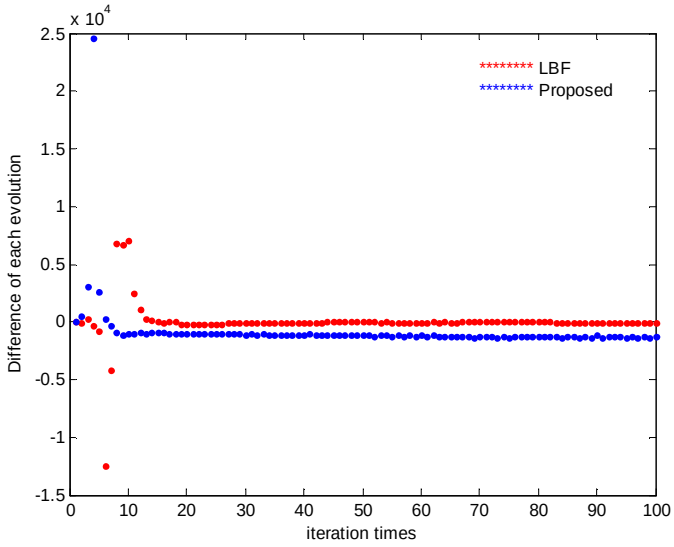

Fig.4 The comparison of the convergence of different algorithms, the initial contour is as the second row of Fig.3, the iteration times is 100

4.3 The analysis of the guided gradient

To validate the effect of the proposed algorithm, we reference the different types of images. Because of our algorithm has the ability to find the correct regions, in the experiments, we choose the fixed initial contour. The first two images of Fig.5 are chosen as two-phase images and the image region is single. On this condition, the segment results of our proposed algorithm are better than the other kinds of local based active contour models. For the purpose of comparing the edge covering rate, the following two images are chosen as multi-phase and multi-region.

Seeing from the segmentation results, we may found the proposed gradient guided algorithm is more consistent to the strong edges of the image. Fig.5 shows all the segment results.

CONCLUSION

In this work, we propose a novel framework based on active contour model for image segmentation. The proposed model may efficiently utilizes image gradient and region information, which in certain case has resulted in significant improvement in accuracy and time consuming for segmenting various images with transitional regions and boundaries.

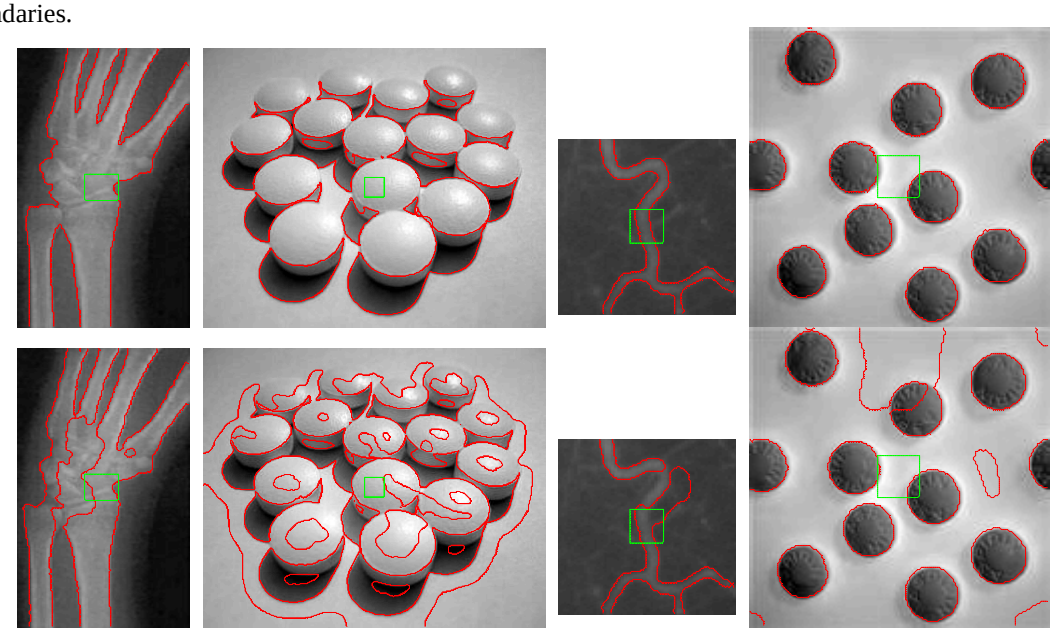

Fig.5 The segmentation results: the first row is the results of the proposed algorithm, the second row is the result of LBF, in all the testing, sigma is set to 4, iteration times are 100

Like all of the active contour based segmentation models, the parameter of our model is also an important problem. In our algorithm, the image are roughly divided into two region inner pixels and region edge pixels, but the choosing of the threshold between the different gradients is very difficult. The fix value would not fit different input images. For the purpose of letting the algorithm more adaptable, the dividing of the gradient should be adjusted according to the input image, or even based on the different image regions. In the following works, the study of the local and global adaptable dividing would be our main works.

Acknowledgements
The authors thank the anonymous reviewers for their many valuable comments and suggestions that helped to improve both the technical content and the presentation quality of this paper.

REFERENCES

[1] Q. Zheng, E. Dong, Z. Cao, W. Sun, and Z. Li, *Signal Processing*, vol. 97, pp. 117-133, **2014**.
[2] W. Wang, L. Zhu, J. Qin, Y.-P. Chui, B. N. Li, and P.-A. Heng, *Optics and Lasers in Engineering*, vol. 54, pp. 105-116, **2014**.
[3] Q. ZHENG and E.-Q. DONG, *Acta Astronautica Sinica*, vol. 39, pp. 21-30, **2013**.
[4] X. Xie, J. Wu, and M. Jing, *Pattern Recognition Letters*, 2013.
[5] Y. Wu, Y. Wang, and Y. Jia, *Computer Vision and Image Understanding*, **2013**.
[6] D. Li, W. Li, and Q. Liao, *Journal of Visual Communication and Image Representation*, vol. 24, pp. 522-533, **2013**.
[7] L. Wang, C. Li, Q. Sun, D. Xia, and C.-Y. Kao, *Computerized medical imaging and graphics*, vol. 33(7), pp. 520-531, **2009**.
[8] S. Lankton and A. Tannenbaum, *Image Processing, IEEE Transactions on*, vol. 17, pp. 2029-2039, **2008**.
[9] L. Fang and X. Wang, *Optik - International Journal for Light and Electron Optics*, **2013**.
[10] W. Liu, Y. Shang, and X. Yang, *Pattern Recognition Letters*, vol. 34, pp. 655-662, **2013**.
[11] Q. Ge, L. Xiao, H. Huang, and Z. H. Wei, *Digital Signal Processing*, vol. 23, pp. 238-243, **2013**.
[12] T. F. Chan and L. A. Vese, *Image Processing, IEEE Transactions on* vol. 10, pp. 266-277, **2001**.

[13] A. Kovacs and T. Sziranyi, *Pattern Recognition Letters,* vol. 33, pp. 1180-1187, **2012**.
[14] Y. Yang and B. Wu, *Journal of Mathematical Analysis and Applications,* vol. 389, pp. 351-366, **2012**.
[15] C.-y. Yu, W.-s. Zhang, Y.-y. Yu, and Y. Li, *Computers & Mathematics with Applications,* **2013**.
[16] H. Zhou, X. Li, G. Schaefer, M. E. Celebi, and P. Miller, *Computer Vision and Image Understanding,* vol. 117, pp. 1004-1016, **2013**.
[17] C. Li, C.-Y. Kao, J. C. Gore, and Z. Ding, *Image Processing, IEEE Transactions on* vol. 17, pp. 1940-1949, **2008**.
[18] Z. Liu, L. Shen, and Z. Zhang, *Signal Processing,* vol. 91, pp. 290-299, **2011**.
[19] J.-W. Han, Suryanto, J.-H. Kim, S. Sull, and S.-J. Ko, *Digital Signal Processing,* vol. 23, pp. 110-117, **2013**.
[20] L. Wang and C. Pan, *Pattern Recognition,* vol. 47, pp. 1917-1925, **2014**.
[21] V. Kumar, J. K. Chhabra, and D. Kumar, *Engineering Applications of Artificial Intelligence,* vol. 29, pp. 93-103, **2014**.